A Variable Radius Roll Adhesion Test (VaRRAT) Suitable for Measuring The Adhesion of Paint to Metal

Damien Jinks, Hugh Brown, and David Buxton†—University of Wollongong*

Early trials and analysis of a new adhesion test are discussed. The test is designed for measuring the adhesion of paint to deformable steel sheets as used in building, automotive, and other cladding applications, and does not require detailed knowledge of the paint mechanical properties. A stiff overlay, such as an epoxy resin, is applied to the coating, and the steel substrate is peeled away using a roll of well-defined radius to which the steel substrate is constrained. The propagation of a crack within the paint or at some interface in the paint/metal system depends mostly on the mechanical properties and thickness of the overlay and the radius of the constraining roll. The test is shown to discriminate better than existing practical adhesion tests between paints of expected differing adhesion/cohesion, but also presents some inconsistencies that require further work to resolve.

INTRODUCTION

Organic coated formable metallic sheets are used extensively as cladding in automotive and building applications. As part of product quality control and product development, it is desirable to measure adhesion in these painted metal systems. Unfortunately, the choice of adhesion test and the interpretation of its results is not always a trivial matter. In practice, "practical" adhesion tests tend to be relied upon. Examples of these would include the cross-hatch style of test, the reverse impact test, and the T-bend test. Practical adhesion tests are distinguished from fracture mechanics-based tests in that often they relate to the service use of the coating system, are quick and easy to perform, and are easy to analyze. By contrast, fracture mechanics-based tests usually require the preparation of special fracture specimens, precise measurements of loads or displacements, and good knowledge of relevant material properties in order for a specimen independent measure of adhesion to be performed.

The advantage of fracture mechanics-based tests is that they enable meaningful comparisons to be made between results of tests where differing materials or geometries are utilized. In general, practical adhesion tests do not consider the specific material properties or dimensions in determining a result, and hence these factors may confound the result of the test. It is for this reason of deconvolution that there is a significant motivation to develop adhesion tests based on fracture mechanics principles which are suitable for the systems of interest, and are relatively simple to perform and analyze.

The key difficulties for developing good fracture tests for paint films relates to their high adhesion, their cohesive toughness, and uncertainty regarding their mechanical properties. For example, in attempting to measure the mechanical properties of epoxy resins on aluminum and titanium substrates, Roche et al. found that their measured coating mechanical properties were dependent on film thickness, cure conditions, substrate material, and substrate surface treatment.[1]

Fracture mechanics-based tests have been applied to paint coatings on metal, most of them based on the blister test configuration.[2,3] In the blister test first proposed by Dannenberg,[3] the base of the coating is exposed through a hole in the substrate into which a fluid is injected under pressure (*Figure* 1). The fluid forces the coating to form a blister and ideally, at some critical pressure, the coating at the edge of the blister delaminates and the radius of the blister increases. The test is not without its difficulties and tends not to work well in its standard form for the paint coating systems of interest because the paint is cohesively weak in comparison to the adhesion, and fails before the blister can be propagated.[4] This problem is made worse by the mode mixity at the crack tip, which is such that it is

*BHP Institute of Steel Processing and Products, Wollongong NSW 2522, Australia; email: hugh_brown@uow.edu.au.
†BHP Coated Steel Research Laboratories, P.O. Box 1854, Wollongong NSW 2500, Australia; buxton.david.db@bhp.com.au.

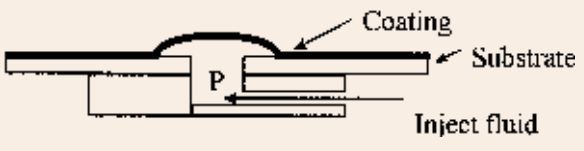

Figure 1—Standard blister test configuration.

energetically favorable for the crack to propagate toward the coating rather than the substrate. Also, there is an occasional tendency toward axisymmetric crack propagation, making the estimation of the crack radius difficult.[4]

A variation of the blister test that addresses the issue of weak coatings is the inverted blister test. Here the coating is adhered to a stiff substrate, and what was formerly the substrate becomes the blister layer. Fernando et al.[2] used the inverted blister test in a limited study to measure the adhesion between the 50 μm thick steel shim and electrocoated amino/epoxy-based paint. When blistering thicker steel substrates it becomes more difficult to implement the inverted blister test because as the pressures increase, the deflections become smaller (of the order of 0.2 mm for the system studied), and the crack radius after initial propagation becomes more difficult to estimate.

Meth et al. recently have applied a laser induced decohesion blister test to metal/polymer systems.[5] A laser pulse is applied to the side of the coating which consists of an automotive clearcoat over some basecoat. The layer under the clearcoat is ablated by the laser pulse, thus forming a blister on the topcoat which may be analyzed in a similar fashion to the blister test. Obviously, the laser spallation technique is limited to interfaces where there is a sufficient optically transparent topcoat. Meth et al. presumed that the failure plane is within the top few microns of the basecoat and so it is really cohesive failure rather than adhesive failure which is being measured. The results show a clear trend with adhesion energies ranging from 44 J/m^2 for white basecoat to 740 J/m^2 for black basecoat, which is consistent with the trend in pigment to resin ratios of the measured basecoats. The laser ablation technique provides some of the few paint fracture measurements available for comparison with our test. It is interesting to note that no problems with topcoat failure were reported, contrary to experience with conventional blister tests. This may be attributed to the nature of the crack driving force where there is maximum pressure when there is material being ablated on one of the crack faces. If the crack deviates upwards into the clear topcoat, then the local pressure at the crack tip may be reduced as there is no longer ablation occurring on one crack face.

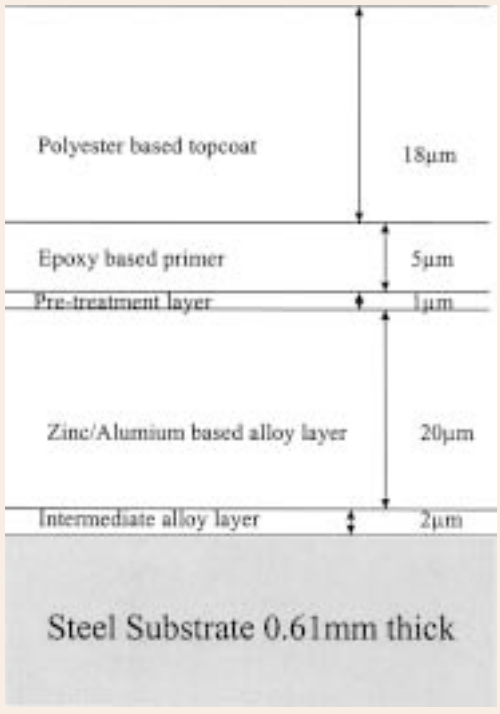

Figure 2—The coating system of interest.

This paper reports background, analysis, and early experimental results from a new fracture mechanics-based adhesion test used to measure paint adhesion to painted steel sheets thus avoiding the need for good mechanical data for the coating. The system examined in this study consists of a zinc/aluminum alloy coated steel sheet coated with an epoxy-based primer and a polyester-based topcoat (*Figure* 2).

DESCRIPTION AND BACKGROUND OF THE TEST

A diagram of the proposed test geometry is shown in *Figure* 3, and a photograph of the test is given in *Figure* 4. The test relies on the application of a reinforcing layer of epoxy resin over the painted side of a narrow strip of the coated metal (zinc/aluminum alloy coated steel is used in this study). The sample is locked into the roll at the low radius of curvature section and the steel substrate is "rolled" away from the epoxy resin propagating a crack somewhere within the paint system, or at an interface. The loading configuration drives the crack preferentially toward the steel rather than into the epoxy resin[6] while the epoxy resin overlay provides sufficient stiffness to cause the crack to propagate when the steel is rolled around an appropriate radius. The mode mixity has been estimated by finite element techniques for just one roll radius and epoxy thickness to be quite small, 3.6°, but in the direction to drive the crack towards the steel. This analysis will be the subject of a later paper.

There are two obvious potential adhesion measurements in such a system, critical roll radius and critical epoxy resin thickness. It was felt that measuring by roll radius would reduce the required amount of sample preparation if a variable radius roll were used. An involute curve was the shape used for three specially machined rolls with variable radius of curvature. The variable radius roll permits an adhesion measurement from each sample. The crack is initiated at the very small radii presented by the start of the curve. The crack propagates around steadily increasing radii until it finds some critical radius at which insufficient energy is stored in the epoxy resin to drive it further. This radius is the "critical radius" for the sample and represents an adhesion measurement where smaller critical radii represent stronger

adhesion energies. It is worth noting that, for steady crack propagation, this test measures a crack arrest adhesion energy. Normally, fracture mechanics tests measure a crack propagation energy or a crack initiation energy. At the time of writing, the test is "driven" by hand and interpreted by "eye." However, there is no fundamental reason why automation could not be used to make the test more consistent.

Unfortunately, the epoxy resin has relatively complex mechanical properties, so any mechanical analysis of the test requires at least some elastic-plastic properties to be included. Other, more mechanically linear-elastic, overlays were tested, but they resulted in consistent failure between the epoxy resin and the overlay rather than within the paint or at an interface of interest. It would have been desirable for the overlay to be linear-elastic over the expected loading range, but the epoxy resin simply worked better than the other materials at reliably producing failures at the interfaces of interest in a mechanically straightforward manner. The test should be distinguished from a peel style test, in that while a peeling action is occurring no attempt is made to measure the peeling force.

The design for the variable radius roll adhesion test (VaRRAT) was derived after considering variations of existing adhesive joint tests such as the double cantilever and lap shear tests.

Double cantilever style tests have been used to measure the adhesion of epoxy-aluminum joints[7] and have been used to study the adhesion in polymer-nonpolymer interfaces where the interfaces have been modified by diblock copolymers.[8] In both of these studies, mode mixity has been related to the interface of failure. In order to adapt the system of interest to double cantilever style tests, aluminum beams were adhered to the samples to provide stiffness. Two types of specimen were prepared. The first consisted of the underside of the steel adhered to one beam, and the coated side of the sample adhered to the second beam. The second type was symmetrical, with two samples each adhered to a beam at the base of the steel, with the coated sides of the two samples adhered at the middle. The samples were tested on a double cantilever rig capable of generating a wide range of mode mixities at the crack tip. The design of the rig was quite similar to that described by Fernlund and Spelt.[9] When applied to the specimens studied, failures were found to occur between the aluminum and the epoxy, as in the case of the asymmetrical specimen. For the symmetrical specimens, failures occurred mostly between the topcoat and epoxy, seemingly independent of the applied mode mixity. It was concluded that, despite significant mode II being present, there was little crack driving force toward the steel substrate.

The lap shear specimen is a standard configuration and the failure stress or energy of this specimen is frequently given as a specification of adhesive strength. While it is commonly used as a practical adhesion test, it is possible to extract fracture mechanics information as long as the crack tip is well defined. A range of different lap shear type specimens was prepared and tested including two samples adhered together, the sample used as tensile specimen with a stiff overlay and preinitiated crack, and a range of reinforced versions of these. Care was taken to

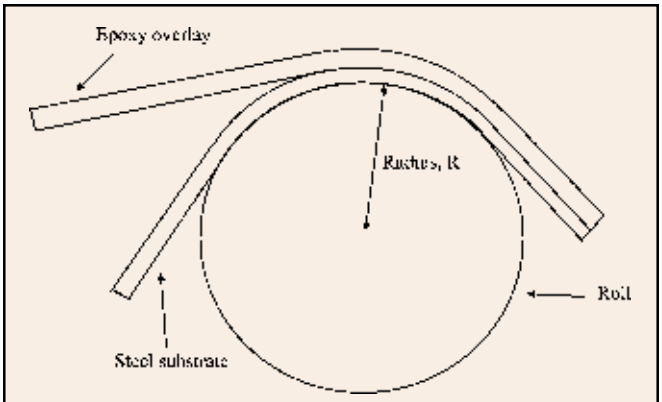

Figure 3—Conceptual test geometry.

initiate the cracks before loading. The most straightforward manner of initiating the crack when an overlay was present was simply to bend the substrate. Usually, the lifting of the overlay would expose some of the substrate or interior of the paint system. The general problem with these tests was that failure occurred either at the adhesive topcoat interface or the adhesive "additional adherand" interface, or that the steel substrate would break before a crack could be propagated.

Peel tests were also considered. In order to drive the crack toward the steel and to protect the paint from failure, the substrate was peeled off the coating rather than the coating peeled from the substrate. The paint coating was adhered to a stiff substrate and the steel was pulled off. It was found that crack propagation was very inconsistent, with failure tending to occur between the epoxy and the topcoat, or in the paint system. When failure occurred in the paint the fracture surface was patchy. Also, plastic deformation of the steel tended to occur in an uncontrolled manner, making any potential analysis of the test difficult. Therefore, the peel test was also rejected.

Based on the above work, the following general observations were made.

(1) For the system of interest, bending the substrate works well to initiate the crack in the presence of an epoxy resin overlay.

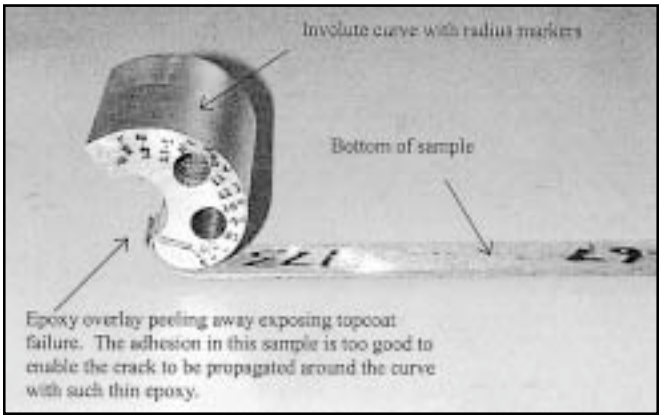

Figure 4—Photograph of test using a roll of variable radius of curvature.

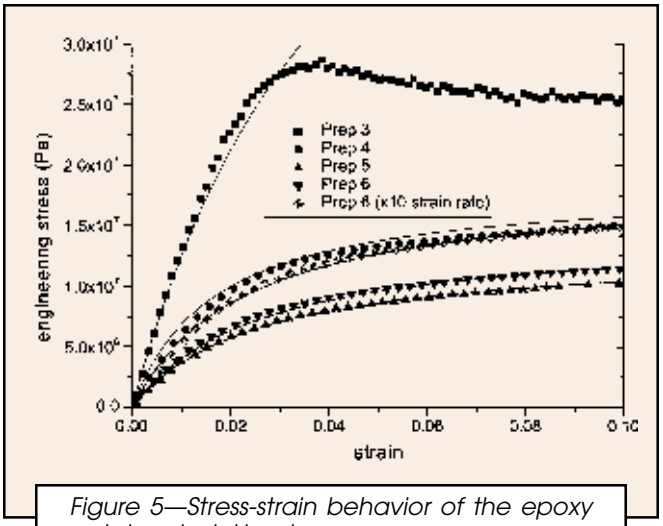

Figure 5—Stress-strain behavior of the epoxy resin in uniaxial tension.

(2) Independent of the overlay applied to the coating, applying tension alone to the steel substrate will not propagate the crack, as the substrate will tend to break before propagation occurs.

(3) An epoxy resin applied thickly can be used to initiate and propagate a crack by bending the substrate, but it will readily delaminate from the topcoat if it is in turn connected to a stiffer adherand such as an aluminum beam.

While not having proven that the previously discussed test configurations could not have been adapted with further efforts to the system of interest, we concluded that the most promising paint adhesion test configuration would use an epoxy resin overlay and have substrate bending as the primary loading method. A practical paint adhesion test with a similar loading configuration was reported by Roche et al.[10] Here, paint adhesion was tested using a three-point flexure test with epoxy resin stiffener.

EXPERIMENTAL

Method and Experimental Design

Strips of the painted sheet metal were cut to required dimensions, and then wiped clean with methanol. They were then laid flat in a polyethylene tray. Ciba-Geigy K106 epoxy resin was poured over the sample, and the tray was placed in an oven set to 70°C for two hours. After curing, the epoxy resin slab containing the samples was removed for machining to the required dimensions.

A factorial experiment design was used to assess the effects of a range of variables on the adhesion measurements. The independent variables were a paint system (three levels), sample width (three levels), epoxy resin thickness (three levels), and epoxy resin batch (two levels). A part factorial design was considered, but it was felt that the possibility of noisy or incomplete data was sufficiently high to merit the additional sample preparation work. The larger number of samples also presented the opportunity to test for the effect of variations in the curing process and the epoxy resin batch.

In summary, the epoxy resin thickness was 1, 2, and 3 mm, the sample width was 20, 30, and 40 mm, the paint topcoat color was white, green, and "sabotaged" green, and the epoxy resin was Ciba Geigy (two-part epoxy) K106 batch #678279 (Batch A) and K106 batch #679046 (Batch B).

The sample systems consisted of a substrate of 0.61 mm thick steel sheet, coated first with 20 μm of zinc/aluminum alloy, then 5 μm of epoxy-based primer, and finally 18 μm of polyester-based topcoat. The two colors represent a low resin/pigment ratio system (white) and a high resin/pigment system (green). The "sabotaged" green had no pretreatment layer between the primer and metal alloy layer (normally associated with poor adhesion), and the system was grossly "over-cured" after application of the topcoat. All three systems met commercial specifications for adhesion, as determined by reverse impact and T-bend tests.

The described experiment, when implemented in a full factorial design, provides 54 samples. Because the curing oven was not large enough to process all the samples in one run, the samples were prepared over several runs. The samples were split up according to epoxy resin batch (27 samples for each epoxy batch). Each list of 27 was then randomly organized, then split into two separate preparations. Each preparation was further split to fit into the top and bottom trays of the oven, again in a random manner.

While the oven was set to 70°C, with the large thermal mass in the oven (approximately 800 g of epoxy resin was used in each preparation), the temperature overshot to 115°C in the first preparation, and to 85°C for the remaining three of the preparations. High temperature cure of the epoxy resin overlay resulted in a thermal mismatch stress when the samples cooled, due to the differing thermal expansion coefficients of the steel and the epoxy resin. The first stage of testing consisted of measuring the radius of curvature of the sample. The second stage was to measure the critical radius where a crack could not be propagated.

Measurement of the Critical Radius

The critical radius measurement is quite simple to perform. The sample is locked into the beginning section of the roll, and the crack is initiated as the sample is stretched over the sharp edge. The sample was pulled around the

Table 1—Fitted Parameters Characterizing Epoxy Resin Mechanical Properties

Preparation	Epoxy Resin Batch	E (Pa) Young's Modulus	D, Shape Factor	E/D (Pa), Approx. Maximum Stress	Comment
3	A	1.505×10^9	21.2	71×10^6	Oven overshot to 115°C. Only applicable to 0.03 strain.
4	A	1.085×10^9	59.1	18×10^6	Slightly less epoxy resin used in batch.
5	B	0.512×10^9	39.4	13×10^6	
6	B	0.564×10^9	38.9	14×10^6	
6	B	0.801×10^9	43.3	18×10^6	10X strain rate

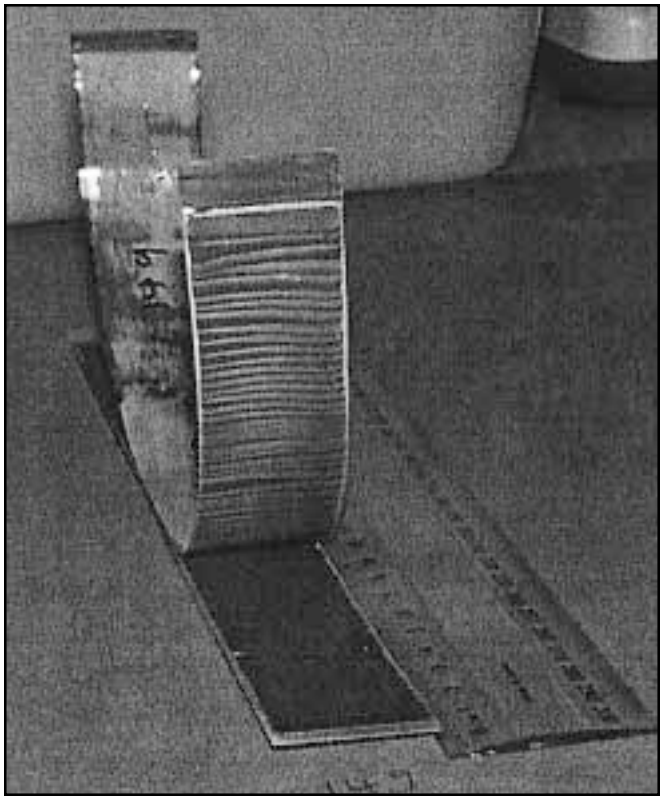

Figure 6—Fracture surface of green from preparation 3.

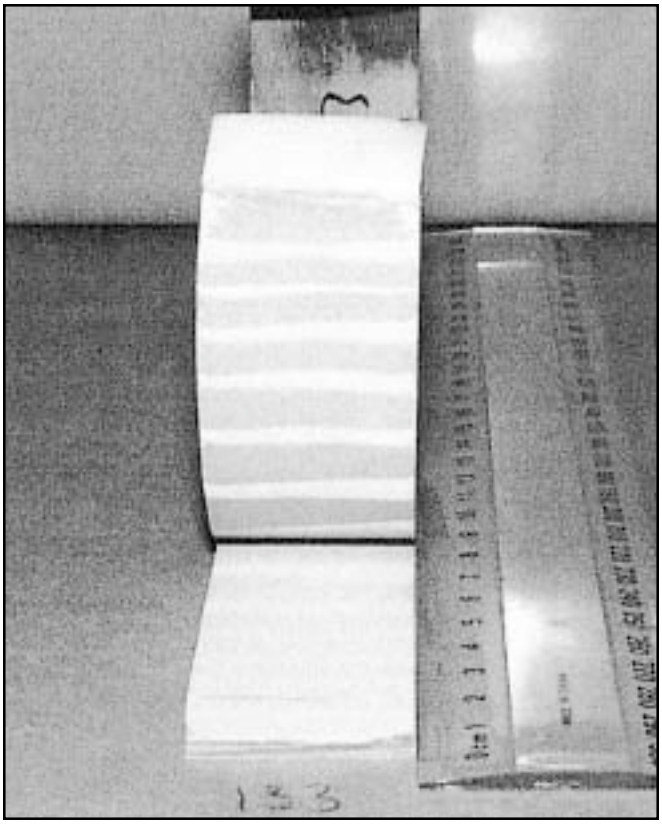

Figure 7—Typical fracture surface of white.

curve by hand, applying enough tension to keep the sample from visibly lifting off the surface of the roll. When sample lift-off occurs, the result becomes less accurate. At the point where the crack stops propagating, the critical radius was read off the edge of the roll. In some cases a crack did not initiate on a particular roll, or continued to propagate beyond the end of the roll. In such a case, only a limiting critical radius was recorded.

In many cases, multiple measurements per sample were achieved. As the results ranged in measurement quality, a statistical weighting system was implemented, which allowed different weightings to be associated with differing precision measurements. A weighting between 1 and 3 was given to each measurement and the measurements were then averaged. Results with weightings of 2 or 3 had two or three times the weight of results with a weight of 1.

Sometimes the sample would hold to the surface of the roll, and the crack would propagate relatively smoothly. In such a case the assumptions made in the mathematical model of the test would hold reasonably well, and the calculated adhesion value should be relatively believable. Results of this sort were given a weight of 3.

On some occasions, the steel strip would lift slightly from the surface of the roll, especially near the crack tip, or the crack would propagate in a stop-start fashion in jumps of several millimeters. Measurements where this was observed were given a weight of 2.

If significant lifting was observed near the crack tip, or the cracks jumped distances of more than 1 cm, then the result was given a weight of 1.

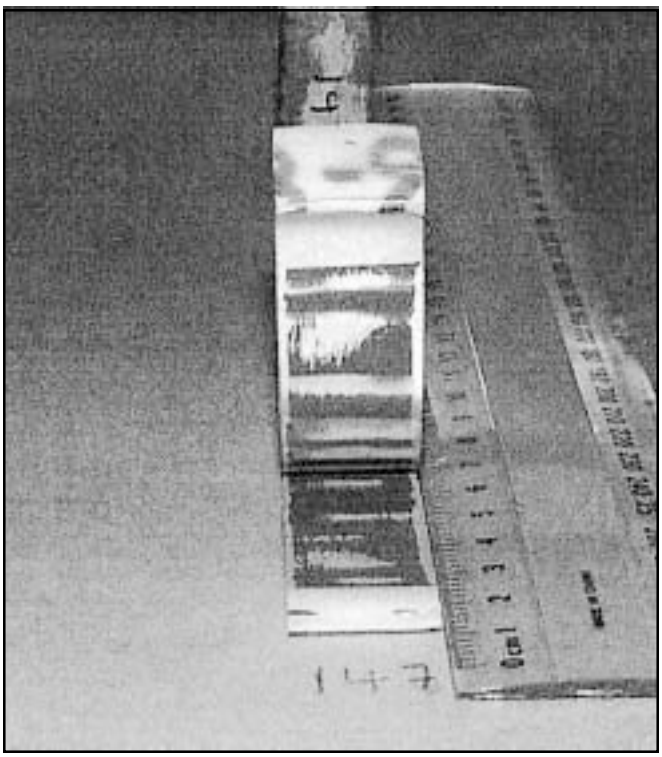

Figure 8—Typical fracture surface of "sabotaged" green.

Table 2—FTIR Results

Paint	"Naked Eye" Observed FailurePlane	Side	Epoxy Detected?	Polyester Detected?	Comments
"Sabotaged" green	Within topcoat	Epoxy resin overlay side	No	Yes	
	Primer/metal	Epoxy resin overlay side	Yes	No	
	Primer/metal	Metal side	Possibly	No	
White	Within topcoat	Epoxy resin overlay side	No	Yes	
	Within topcoat	Metal side	No	Yes	V. poor signal
	Primer/topcoat	Epoxy resin overlay side	No	Yes	
	Primer/topcoat	Metal side	Yes	Possibly	
Green	Within topcoat	Epoxy resin overlay side	No	Yes	

Mechanical Properties of the Epoxy Resin

In order to estimate the adhesion energy, measurement of the epoxy resin mechanical properties was required. Stress strain curves were taken using a selection of removed 3 mm epoxy resin overlays. At 3 mm these were the thickest samples available, and therefore the least "prestrained" by adhesion testing.

The mechanical properties of the epoxy resin were measured under uniaxial tension up to a strain of 0.1, at a strain rate of 3%/min. Strains were estimated from the crosshead positions. No Poisson's ratio measurement was performed. Sample necking was not found to be significant, so little error in stress measurement was expected due to the change in the cross-sectional area of the sample during mechanical testing.

For the purpose of applying the data to a model, the mechanical data was fitted using a classic relation

$$\sigma = E\frac{\varepsilon}{1+D\varepsilon}$$

where σ is stress (Pa) and ε is engineering strain. E and D are fitted parameters where E is a magnitude (in Pa) equal to the Young's modulus at low strain, and D is a shape factor describing the shape of the stress-strain curve. The stress and strain are in terms of engineering stress and nominal strain. A conversion into true stress is expected to make a difference of up to about 3% for the ultimate stress of the epoxy resin.

More complicated equations that fit the data better could have been used, but it was felt that insufficient additional accuracy was obtained by their use, and the additional parameters when fitted tended to vary in a random manner making the relation of the fitted parameters to the results of the adhesion test unreliable.

Plots of typical stress-strain curves are given in *Figure* 5. The data was fitted using the above stress-strain equation with acceptable results, except for data from preparation 3 which had to be truncated to about 0.03 strain. Beyond this strain the data indicated a much more sudden yielding (and perhaps necking) than for the other preparations, making application of the model in cases where epoxy resin strain extended beyond 0.03 inaccurate. The fitted parameters are given in *Table* 1.

RESULTS

Fracture Surfaces

The green topcoat paint system tended to fail consistently somewhere within the topcoat when failure occurred at low critical radius, revealing an even green topcoat surface on both sides. The exceptions to this behavior were the results from preparation 3, and when the critical radius was larger (usually associated with thicker epoxy resin) and an oscillating pattern was observed (*Figure* 6), consistent with start-stop crack propagation. It is believed that during loading, the crack initially penetrates to near the primer layer, then after propagating some distance jumps to somewhere in the topcoat where it would travel a short distance before stopping. The precise mechanisms involved in this process are not well understood at this stage.

The white topcoat consistently displayed the oscillations seen in the preparation 3 green samples, with the exposed primer surface appearing to be much cleaner (*Figure* 7).

The "sabotaged" green displayed the most uneven failures, with patchy sections of exposed metal, primer, and topcoat (*Figure* 8). In preparation 3, when thicker epoxy resin was used, an oscillating pattern similar to that observed for the green was seen.

There was a concern that the plane of fracture was being influenced by diffusion of epoxy from the overlay

Table 3—Data From Regression Analysis[a]

Model	% Variance Explained	INT	Thick	Green	SAB	Batch	Prep5	Tray	DF	RMS Error[b]
1 (Rc)	85.5%	–6.1 not sig.	13.5 strong	–8.4 strong	3.6 not sig.	8.7 medium	1.9 not sig.	–2.8 not sig.	20	4.2
2 (Gc)	88.4%	75.9 low	90.7 strong	63.0 strong	–30.0 low	–32.6 low	–44.7 medium	27.1 low	20	25.7

(a) Strong significance ($p<0.001$), medium significance ($0.001<p<0.01$), low significance ($0.01<p<0.05$), maybe significant ($0.05<p<0.1$), not significant ($p>0.1$).
(b) RMS Error = (loss function / DF)$^{1/2}$, where DF is the number of degrees of freedom in the model, and the loss function is the least squares sum of residials

Table 4—"Apples with Apples" Comparison

Hypothesis	Rc Green > Rc White	Rc White > Rc Sabotaged Green (Including 1 mm Thick Epoxy Data)	Rc White > Rc Sabotaged Green (Excluding 1 mm Thick Epoxy Data)	Re White > Rc Sabotaged Green (Only 1 mm Epoxy Data)
Success rate (y ..... successes/n attempts)	32/32	22/30	22/22	2/8
Probability of ≥ y ..... successes out of n attempts if P (a>b)=0.5 for each attempt	2.3×10^{-10}	0.0081	2.4×10^{-7}	0.965
	Strong sig.	Medium sig.	Strong sig.	Maybe sig.

into the topcoat. The plane of failure within the topcoat might simply be the plane where the concentration of diffused epoxy becomes sufficiently low. To test this hypothesis, Fourier transform infrared spectroscopy (FTIR) in attenuated total reflection mode was performed on several fracture surfaces. In this mode, an incident beam is propagated through an internal reflection element that is in contact with the fracture surface of interest. Multiple internal reflections occur along the length of the element between the top of the element and the element base that is in contact with the fracture surface of interest. Along the base of the element, an evanescent wave propagates into the sample normal to the surface to a depth of 1 μm, allowing the technique to detect the presence of certain chemical groups within this zone.

FTIR was performed at each distinct class of fracture site. In *Table* 2 the general results of the FTIR work are presented. The table lists the failure as interpreted by the naked eye, and then gives the species detected by FTIR for that plane. It should be noted that the spectra generally had poor signal to noise ratios, so that not detecting a species by FTIR does not conclusively demonstrate that it is not present. However, the results suggest that the naked eye can be trusted when interpreting the fracture planes. When looking at the overlay side of a fracture plane, what appears to be topcoat generally is topcoat. When looking at the metal side of a fracture plane, what is thought to be primer or metal is primer or metal, although a small amount of epoxy primer (in the case of a metal surface) or polyester topcoat (in the case of a primer surface) may be present.

Roll Test Adhesion Measurements

A large range of critical radii was recorded with a significant number of results outside the measurable ranges. While these were recorded as $R_c<X$ or $R_c>X$, the analysis of the data containing such numbers presented a difficulty and it was decided that for the purpose of numerical data analysis that they should not be included. The results for the "over-cured" preparation were quite different from those obtained from the other preparations and so, for the purpose of generating a fair measurement of true batch and preparation variability, this data should also be ignored. Furthermore, we could not be certain that any additional curing effect on the paint would be negligible at this higher temperature. There were only two 1 mm epoxy resin thickness samples remaining after this exercise, so they too were removed from the data set. The resultant 27 item data set after the elimination process was insufficient for a standard analysis of a full factorial experiment design. Therefore, a regression technique was used to fit the data set. It should be noted that most of those 27 items represent weighted averages rather than single measurements.

The regression models were of the form:

$$adhesion = INTERCEPT+THICKO\cdot thickness+GREENCO\cdot[Paint=Green]+SABCO\cdot[Paint=Sabotaged\_Green]+BATCHO\cdot[prep=4]+PREPCO\cdot[prep=5]+TRAYCO\cdot[tray=bottom]$$

where capitalized parameters are the fitted coefficients, and lower-case parameters are experimental variables. [X=Y] is a logical operator, such that when X=Y is true, [X=Y]=1, else [X=Y]=0. The dependent variable, adhesion, is either the critical radius or the adhesion energy as calculated using the experimental parameters and a mathematical model. The "base case" is a white, 0 mm epoxy resin thickness sample from the top tray in preparation 6. The adhesion of this base case is equal to INTERCEPT. The regression models were fitted using a standard least squares approach.

Initial studies showed that width was not a significant parameter, so no results for the width effect are presented here. The effect of including residual stress improved the variance explained (R^2) of the adhesion energy models

Table 5—Results of Standard Adhesion Tests on Coatings

	T-Bend Test (% Paint Removal/% Paint Cracking)							T-Bend Test Result	Rev. Impact (Joules)	2 mm (J/m² (95 % CI)
	0T	1T	2T	3T	4T	5T	6T			
Sabotaged green	80/100	80/ 90	60/70	20/50	0/ 10	0/ 0	—	4T	>20	227(51)
White	0/ 90	0/ 90	0/ 80	0/ 70	0/ 60	0/ 20	0/ 0	0T	>20	257(51)
Green	30/90	10/80	30/50	10/30	0/ 20	0/ 0	—	4T	>20	320(51

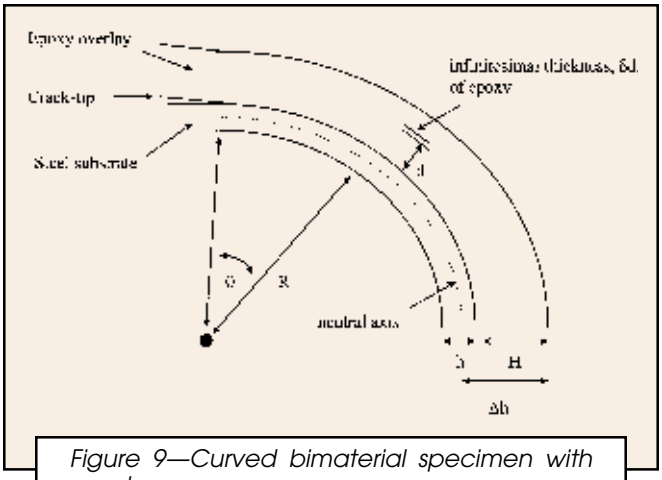

Figure 9—Curved bimaterial specimen with crack.

slightly but did not change any of the basic conclusions. The residual stress adjusted Gc is the value used below. The inclusion of residual stress as a parameter generally increased Gc by about 5 J/m^2, but otherwise changed little.

Results from two regression models are described here, with data from these models presented in *Table* 3.

- In Model 1 it is shown that epoxy resin thickness, paint type, and epoxy resin preparation are significant variables. The residuals for this model do not appear to be random and are probably not "normal," suggesting a systematic effect not included on the model.
- In Model 2, adhesion energy is used as the dependent variable instead of critical radius. Adhesion energy is calculated using the nonlinear elastic plastic epoxy resin material model described later. Here it is found that the relative size of the batch effect is reduced compared to the effect of the paints. However, the effect of preparation alone, which had a low effect in the previous model, has increased substantially, suggesting that the model is overcompensating somehow. The magnitude of the effect of epoxy resin thickness relative to the effect of the paint does not change, also suggesting a possible problem with the adhesion energy model. Tray position becomes a significant variable here indicating that there is some inhomogeneity in the oven temperature. The overall quality of fit parameter R^2 improves from Model 1 to this model, and the systematic variation of the residuals seems to disappear, suggesting that the adhesion energy model accounts for whatever nonrandom factor was not accounted for when critical radius was the dependent variable.

Regression models with interaction terms and with further sub-sets of the data were tested, but were not found to improve the results sufficiently to justify their use, given the limited size of the data sets involved. Nonlinear models were not tested. Attempts were made to further refine the data set by removing the poorer quality measurements as determined by the rating approach used during the experiment. However, the broad conclusions are not changed, and any apparent "improvements" become suspect as smaller data sets are fitted.

While the effect of the sabotaged green paint is of similar order to the RMS error of the fitted models to the data suggesting that the sabotaged green is indistinguishable in adhesion/cohesion effect from the white, a pair-wise comparative analysis does detect a significant difference (*Table* 4). In this analysis, results from the regression analysis have been used to guide the selection of suitable subsets. The subsets consist of comparisons within preparation 3 samples (significant due to overcure) and preparation 4 (significant due to epoxy taken from different batch). Comparisons were allowed between samples from preparations 5 and 6 (same cure and epoxy batch), and within epoxy thickness. Tray position and width were not used to define subsets, so comparisons between samples with differing tray position or width were allowed.

It was found, when considering all possible subsets, that for 22 out of a possible 30 cases where comparison is possible, the sabotaged green has a greater critical radius than the white. Further, all of the cases where the white had a lower critical radius were where the epoxy thickness was 1 mm. This low epoxy thickness was insufficient in many cases to propagate a crack into a measurable region of the roll. This result suggests that the test detects differences in adhesion between the white and the sabotaged green consistently when the epoxy overlay is of sufficient thickness to reliably propagate the crack into the measurable radius region of the roll.

The values of toughness (Gc) for 2 mm thick samples can be obtained from *Table* 3 and the regression model as 257 J/m^2 for white, 320 J/m^2 for green and 227 J/m^2 for sabotaged green. These values are high for toughness, similar to the cohesive toughness of thermoplastics such as polystyrene, and some epoxies, and therefore demonstrate why the adhesion of these paints is difficult to measure.

Performance of Coatings Compared to Conventional "Practical" Adhesion Tests

For the purpose of comparison, conventional adhesion tests were performed with the results given in *Table* 5. From the practical adhesion test data it would normally be said that the white displays the best adhesion, with the green and sabotaged green performing equally poorly. However, the results generated in this study suggest that the order is quite different. The roll test measurements of

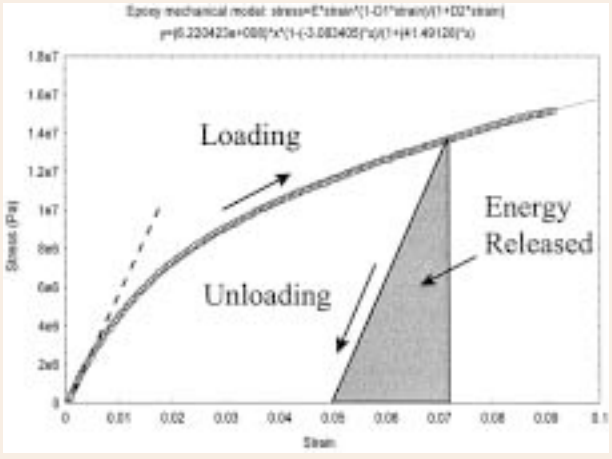

Figure 10—Energy release model for the epoxy resin overlay subject to plane stress.

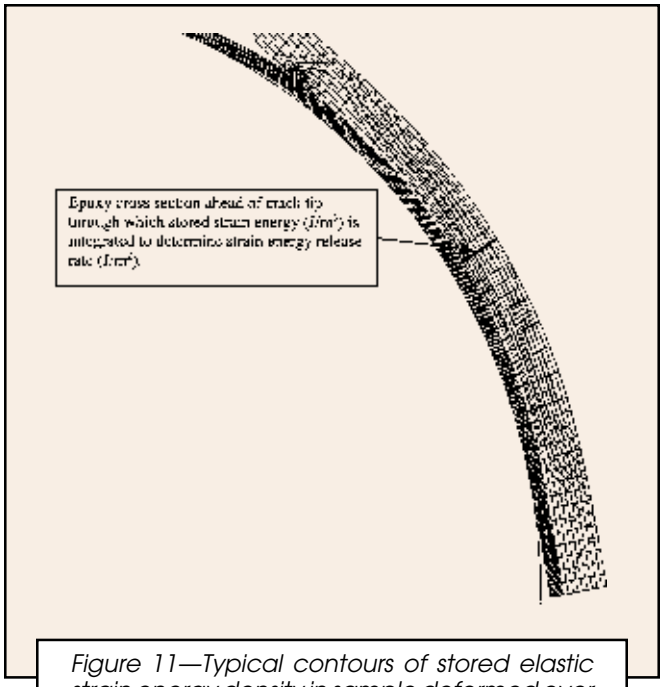

Figure 11—Typical contours of stored elastic strain energy density in sample deformed over roll.

Gc are shown with 95% confidence intervals calculated using the separate regression models for 2 mm, as described above.

MATHEMATICAL MODELING OF THE TEST

General Approach

Analytical and finite element models were constructed in order to calculate adhesion energy from the critical roll radius. Both adhesion test models are based on the assumption that at some distance ahead and behind the crack tip is a uniformly deformed section of sample whose stored strain energy is mostly determined by the sample's state of bending and not influenced by the presence of a complicated crack-tip stress field. When the crack propagates, the uniformly deformed section ahead of the crack tip is shortened and the uniformly deformed section behind the crack tip is lengthened, while little or no energy is added or removed from the region around the crack tip zone as it moves. The argument is not a new one, having been utilized previously for elastic systems by Rivlin et al.[11] Implicit in the argument, as used here, is the assumption that the energy stored in the uniformly deformed section ahead of the crack tip contributes fully to crack propagation in the paint, and is not consumed by plastic deformation by an extended crack tip-field in the epoxy overlay. This is very much a first order assumption which will be addressed in future models. The broad scheme for the models is shown in *Figure* 9. Note that the use of Rice's J-integral[12] calculation is inappropriate for this system due to the large-scale plastic deformation in the overlay (see Appendix for J-integral result).

While the roll used actually has a variable radius, the important feature is that the local radius of curvature varies slowly enough such that the complicated stress field near the crack tip which is associated with crack propagation is sufficiently similar to the crack tip stress field generated by a uniform roll, and not that there are in fact extended zones of uniform deformation ahead and behind the crack-tip.

Analytical Model

In this calculation we will consider only the energy stored in the epoxy resin, and assume that the steel does not release any energy as the crack propagates. It is straightforward enough to show that the change in elastic energy stored in the steel is small compared to the change in elastic energy stored in the epoxy resin, as the crack propagates.

First we estimate the position of the neutral axis, given by Δh, where the factor Δ is a function of the respective thicknesses and elastic properties of the steel and the epoxy resin. This factor may be calculated in a straightforward way for the linear-elastic case, but probably requires a numerical solution when the system has more complex elastic-plastic properties. The elastic mismatch for our system is very large being in the order of a factor of 200 so the neutral axis is expected to be very close to the center of the steel. The difference in predicted adhesion energy between the assumptions of linear-elastic material properties, and the assumption of a central neutral axis position was estimated to be small so it was felt that the assumption of a central position was sufficient for a simple model, and so Δ was defined as

$$\Delta \approx \frac{H}{h} + \frac{1}{2}$$

where h and H are the respective thicknesses of the steel substrate and the epoxy resin overall. The intermediate paint film and alloy layers are of the order of 40 μm thick and are therefore relatively insignificant.

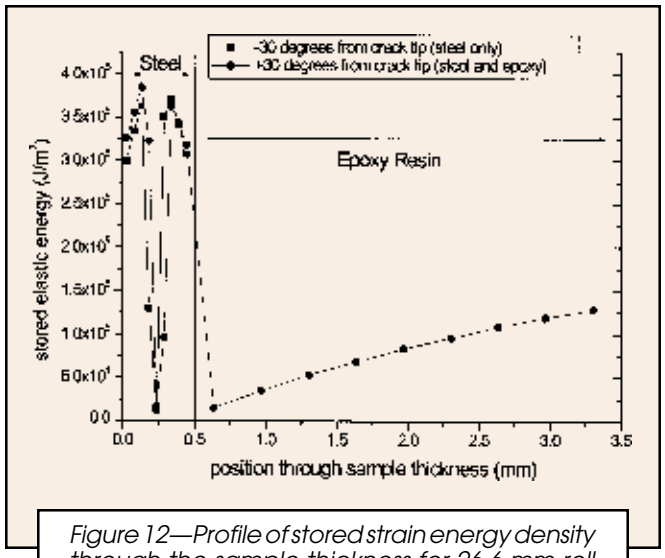

Figure 12—Profile of stored strain energy density through the sample thickness for 26.6 mm roll radius 3 mm epoxy resin thickness sample, at positions –30 ° (-13.9 mm) and +30 ° (13.9 mm) relative to the crack tip.

The strain in the epoxy is therefore given by

$$\varepsilon_x(d) = \left(\frac{\frac{h}{2}+d}{\frac{h}{2}+R}\right), \text{where d varies from 0 to } H$$

It is convenient to define r as the radius of curvature of the neutral axis so $r = R + h/2$.

In practice, we can easily obtain a plane stress-strain tensile curve for the overlay, giving σ(ε) for a simple loading case. The material unloads along some gradient E_u, which we refer to as the unloading modulus. From *Figure* 10 we write the available strain energy density *Ed* for plane stress loading as

$$Ed(\varepsilon) = \frac{\sigma(\varepsilon)^2}{2E_u}$$

For the case of plane strain loading we must solve simultaneously for the contributions from the other principle stress. In the elastic case this gives

$$Ed = \frac{E}{2}\frac{\varepsilon_x^{\,2}}{1-\nu^2}$$

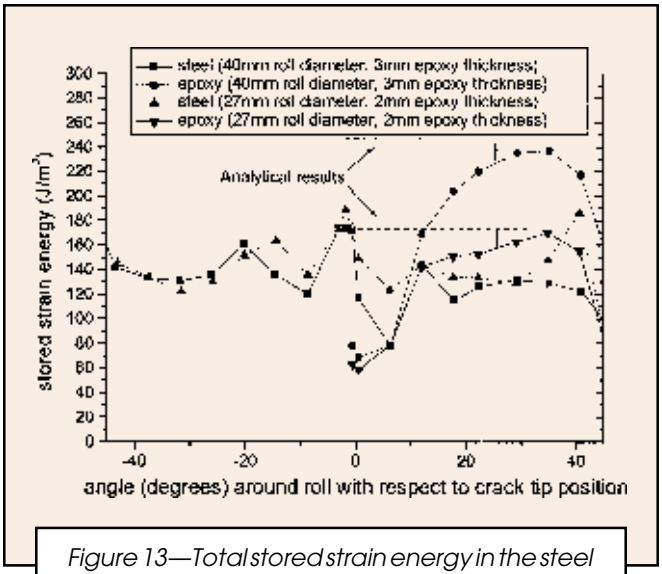

Figure 13—Total stored strain energy in the steel and epoxy resin, as a function of position relative to the crack tip. Analytical model calculates for 26.6 mm roll radius and 2 mm epoxy resin, that G=174J/m², and at 39.6 mm/3 mm, G=247J/m². The angular position allows straightforward comparison between cases with differing roll radii.

In practice, for steel substrates of the order of 0.5 mm thick, and epoxy overlays ranging from 1 to 3 mm thick, the strains are under 5% and the effective Poisson's ratio is less than 1/2, so we are able to make an approximation specific to this model. That is, that we may decouple the energy stored due to the Poisson's contraction resisted under the plane strain assumption, from the energy stored due to the first principle strain due to bending. Using the Tayler series expansion

$$\frac{1}{1-x^2} = 1 + x^2 + x^4 + ... + x^{2n}$$

we may approximate the available strain energy density for the elastic case as

$$Ed = \frac{E\varepsilon^2}{2}(1+\nu^2)$$

or for the elastic-plastic case

$$Ed = \frac{1}{2E_u}(\sigma(\varepsilon)^2 + \sigma(\nu\varepsilon)^2)$$

While under the Mises yield criteria, the plane strain constraint changes the yield strain in the principle bending plane, we assume here that the extent of this change is small.

Recalling the assumption above that the energy released from the steel as the crack propagates is small, we write the strain energy release rate by integrating the above energy density quantity over the thickness of the overlay giving

$$G = \int_0^H Ed_b(d) + Ed_p(d)dd$$

where the *b* and *p* subscripts refer to bending and Poisson's, respectively

or

$$G = \frac{I}{2E_u}\int_0^H \sigma(\varepsilon(d))^2 + \sigma(\nu\cdot\varepsilon(d))^2 dd$$

Explicit solutions may be given for some simple tensile yield curves. In other cases, a numerical integration is required

Case 1: Exponential Strain Hardening

$$\sigma(\varepsilon) = A\cdot\varepsilon^n$$

$$G_b = \frac{A^2}{4E_u(1+2n)}\left(\left(\frac{h+2H}{r}\right)^{2n}\left(\frac{4H}{2^{1+2n}}+\frac{h}{2^{2n}}\right)-\left(\frac{h}{r}\right)^{2n}\left(\frac{h}{2^{2n}}\right)\right)$$

$$G_p = \frac{A^2}{4E_u(1+2n)}\left(\left(\nu\frac{h+2H}{r}\right)^{2n}\left(\frac{4H}{2^{1+2n}}+\frac{h}{2^{2n}}\right)-\left(\nu\frac{h}{r}\right)^{2n}\left(\frac{h}{2^{2n}}\right)\right)$$

where

$$G = G_b + G_p$$

Case 2: Classic Relation:

$$\sigma(\varepsilon) = \frac{E_u \varepsilon}{1 + D\varepsilon}$$

$$G_b = \frac{E^2}{2E_u D^3}\left(\frac{(2DHr + HD^2h + 2D^2H^2 - 2r^2 - (4r^2 + 2rDh + 4rDH)ln(2r + Dh + 2DH))}{(2r + Dh + 2DH} + r\frac{(r + (2r + Dh)ln(2r + Dh)}{(2r + Dh)}\right)$$

$$G_p = \frac{E^2}{2\nu E_u D^3}\left(\frac{(2\nu DHr + \nu^2 HD^2h + 2\nu^2 D^2H^2 - 2r^2 - (4r^2 + 2\nu rDh + 4\nu rDH)ln(2r + \nu Dh + 2\nu DH)}{(2r + \nu Dh + 2\nu DH} + r\frac{(r + (2r + \nu Dh)ln(2r + \nu Dh)}{(2r + \nu Dh)}\right)$$

where

$$G = G_b + G_p$$

Finite Element Models

The finite element models were constructed using the FEM program ABAQUS. The models used four-node plane-strain reduced integration elements for the specimen, and rigid elements for the roll. Nonlinear elastic-plastic material properties were assumed with the epoxy resin yield curves taken from the mechanical data shown earlier. The sample was displaced over the roll under constant tension, and zero friction was assumed between the roll and the sample. No attempt was made to refine the mesh near the crack tip as crack tip stress field accuracy is not required for this calculation.

Two model results are presented here, with the model dimensions chosen from the results of the regression analysis of the experimental data. The regression models were used to calculate the average critical radius, Rc, for the "sabotaged" green paint for the 2 and 3 mm epoxy resin thickness cases of preparation 5 epoxy resin. Ideally Gc should be geometrically independent, so assuming rate effects are small, we might expect these two samples to generate the same Gc. Yet, our analytical model calculated for these two cases differing values of Gc. To test the accuracy of the model assumptions, finite element models were constructed for both these cases and Gc was calculated using the above energy arguments. An example of the deformed mesh is given in *Figure* 11.

Figure 12 shows typical strain energy profiles through the thickness of the sample, ahead and behind the crack tip. These profiles are integrated to give stored energy (in J/m^2) at a range of positions along the strip for both epoxy resin thickness samples (*Figure* 13). There is some small scale lifting of the sample from the roll at the crack tip which probably contributes to the considerable distance of about five times the epoxy resin thickness before the stored strain energy profile becomes smooth. In the finite element models, contact with the roll tended to occur at points separated by distances in the order of several mm generating some additional noise, particularly in the stored elastic energy profiles for the steel. At both radii of curvature, plastic deformation occurred in the steel reducing the effect of the differing radii on the elastic energy stored in the steel. The neutral axis in the FEM was noted to be close to the center of the steel in agreement with the assumption made in the analytical model described earlier. The only difference in energy profile in the more uniformly deformed sections is therefore associated with the epoxy resin, whose stored energy is then representative of the strain energy release rate for the system. In *Figure* 13 the analytical result for the strain energy release rate is marked for each of the cases. It is observed that the peak energies stored in the epoxy resin are only slightly lower than those calculated using the analytical model, suggesting an overall general agreement between the models.

DISCUSSION

The adhesion test results generated a combination of interfacial and cohesive failures and gave the rank order of adhesion/cohesion (for convenience referred to simply as "adhesion") with the green as highest, followed by the white, then closely trailed by the sabotaged green (green > white ≥ sabotaged green). The confidence intervals estimated from the regression analysis suggest that the difference in adhesion between the white paint and the sabotaged green paint is not very significant. However, consideration of the subsets of the data where samples from the same preparation and epoxy resin thickness are compared consistently show the order is as suggested above. The measured order is consistent with the respective pigment to binder ratios of the white and green, and with the fact that the sabotaged sample was seriously compromised during manufacture. A similar dependence on pigment to binder ratio of adhesion energy was observed by Meth et al.[5] along with similar order adhesion numbers, albeit with a broader range of adhesion energies than occurs in this roll test study.

The measured order of adhesion contrasts with that found using more conventional tests, particularly the T-bend test where the white sample was measured as higher in adhesion than the other samples. It should be noted that the T-bend result depends not only on adhesion, but also the stiffness of the coating and its cohesive fracture toughness. It is possible that the earlier cracking of the white paint relieved sufficient stress to prevent delamination at 0T, making it present an apparently higher T-bend adhesion than the other paints which did not crack as readily.

Of the other variables considered using the roll test, sample width was not found to have any significant effect, consistent with assumptions of plane strain. Epoxy resin overlay thickness was most significant, with adhesion energy apparently increasing with thickness. Some batch variability in results was also observed.

The study did not include a detailed assessment of the unloading stress-strain properties of the epoxy resin, and assumed a relatively simple plasticity model. Future studies will require more detailed mechanical data for the epoxy resin and may consider higher epoxy resin cure temperatures to improve the linear-elastic character of the epoxy resin and to reduce batch variability due to small differences in cure regime.

In addition to the effect of the epoxy resin mechanical model on the test result, the issue of the validity of the overall model of the test was considered. For the purpose of simplicity in this preliminary investigation, the model treated the effect of the plane strain lateral constraint in a first order fashion, assumed that the crack tip does not contribute significant additional plastic deformation to the epoxy resin and ignored rate effects. Also, the model assumed that the samples conform to the surface of the roll, where in practice it was noted that there was a tendency when the epoxy resin was thicker for the sample to lift from the roll in the region of the crack tip changing the loading conditions. These factors, when combined with manual loading technique used, may well account for some measured thickness effect. To better address the above issues, a mechanized VaRRAT rig is being built in which loads and rates will be precisely controlled over a large range and a more refined mechanical model is to be considered. In this work with the manual loading, it was not possible to control loading or crack growth rates inspite of the fact that both the adhesion and the mechanical properties of the epoxy are expected to be rate dependent. Effects of rate, obtained with the mechanized rig, will be described in a later publication.

CONCLUSION

A new roll style adhesion test for measuring the adhesion of paint to metal has been described, and early results of its application have been presented. The test detects differences in paint adhesion/cohesion which practical adhesion tests fail to detect. The test also produces consistent modes of failure for each sample class. Sample preparation and adhesion measurement is relatively straightforward and does not rely on knowledge of difficulty to measure paint or other thin film mechanical properties. A mechanical model of the adhesion test has been developed. Adhesion energies predicted by the model are of the right order, but the model fails to fully account for changes in epoxy resin overlay thickness and mechanical properties. These problems are attributed mainly to the simplifying model assumptions, and to poor sample to roll conformation in some cases.

ACKNOWLEDGMENTS

The authors would like to thank Greg Knight of BHP for helpful suggestions regarding the statistical analysis and Victoria Chapman, also from BHP, for assistance with sample preparation and FTIR analysis.

References

(1) Roche, A.A. and Guillemenet, J., "Mechanical and Chemical Properties of Organic Coatings Applied to Metallic Sheet Substrates," *Thin Solid Films*, 342, 52-60 (1999).
(2) Fernando, M. and Kinloch, A.J., "Use of the 'Inverted-Blister' Test to Study the Adhesion of Photopolymers," *Int. J. Adhes. Adhesives*, 10, 69-76 (1990).
(3) Dannenberg, H., *J. Appl. Polym. Sci.*, 5, 125 (1961).
(4) Bessell, S. and Chaffee, A.L., "Evaluation of the Blister Test for Measurement of Adhesion of Organic Coatings on Steel Substrates," *BHPR/SF/N/017* (BHP Research, 1995).
(5) Meth, J.S., Sanderson, D., Mutchler, C., and Bennison, J., "Quantification of Coating Adhesion Using Laser Induced Decohesion Spectroscopy," *J. Adhes.*, 68, 117-142 (1998).
(6) Cao, H.C. and Evans, A.G., "An Experimental Study of the Fracture Resistance of Bimaterial Interfaces," *Mech. of Mater.*, 7, 295-304 (1989).
(7) Fernlund, G., Plausinis, D.J., and Spelt, J.K., "Load Jigs for Mixed-Mode Fracture Testing of Adhesive Joints," Novel Experimental Techniques in Fracture Mechanics, American Society of Mechanical Engineers, Applied Mechanics Division, AMD. Publ by ASME, New York, 35-45 (1993).
(8) Smith, J.W., et al., "The Measurement of the Fracture Toughness of Polymer-Nonpolymer Interfaces," *J. Mater. Sci.*, 28, 4234-44 (1993).
(9) Fernlund, G. and Spelt, J.K. "Mixed-Mode Fracture Characterization of Adhesive Joints," *Composites Science & Technology*, 50, 441-449 (1994).
(10) Roche, A.A., Dole, P., and Bouzziri, M., "Measurement of the Practical Adhesion of Paint Coatings to Metallic Sheets by the Pull-Off and Three-Point Flexure Tests," *J. Adhes. Sci. Tech.*, 8, 587-609 (1994).
(11) Rivlin, R.S. and Thomas, A.G., "Rupture of Rubber. I. Characteristic Energy for Tearing," *J. Polym. Sci.*, 10, 291-318 (1952).
(12) Rice, J.R., Trans. AMSE Ser. E., *J. Appl. Mech.*, 90, 379-386 (1968).

APPENDIX

The J-integral is a method for calculating strain energy release rates for specimens with nonlinear elastic properties proposed by Rice.[12] It is sometimes applied to calculate strain energy release rates for specimens where plastic deformation occurs, but it is not necessarily suitable for such applications. First we present the results of an analytical J-integral calculation using the path shown in *Figure* 14.

The J integral is given by

$$J = \int_{r} W dy - T \frac{\partial u}{\partial x} ds$$

where

Γ is the contour path of the integral enclosing the crack
T is the traction vector acting on the path, given as

$$T_i = \sigma_{ij} n_j$$

where

n_i are direction cosines of the outward normal vector to Γ.
u is a displacement vector
dS and element of arc along Γ
x,y are Cartesian coordinates

and

$$W = W(\varepsilon_{ij}) = \int_{o}^{\varepsilon_{ij}} \sigma_{ij} d\varepsilon_{ij}$$

is the strain energy density, or in the case of an elastic-plastic material, the strain energy density for an equivalent elastic material.

The J-integral may be expanded to:

$$J = \int_{r} \left[W(E_{ij}) n_1 - (\sigma_{11} n_1 + \sigma_{12} n_2) \frac{\partial u_1}{\partial x_1} - (\sigma_{12} n_1 + \sigma_{22} n_2) \frac{\partial u_2}{\partial x_1} \right] dS$$

where

Contour 4 is traction free and does not contribute. Contour 6 approaches zero when a>>H. Thus the J-integral is comprised of:

$$J \approx J_1 + J_2 + J_{3a} + J_{3b}$$

or

$$J \approx \int_{-h}^{0} -\int_{0}^{\varepsilon_{11}} \sigma_{11(X_1=0)}\, d\varepsilon_{11}\, dx_1 + \int_{0}^{l} -\sigma_{22}\frac{\partial u_2}{\partial x_1}\, dx_1 + \int_{-h}^{0}\int_{0}^{\varepsilon_{11}} \sigma_{11(X_1=l)}\, d\varepsilon_{11}\, dx_1 + \int_{0}^{H}\int_{0}^{\varepsilon_{11}} \sigma_{11(X_1=l)}\, d\varepsilon_{11}\, dx_1$$

Contour 2 (J_2), is likely to be small since $\delta u_2/\delta x_1$ is small as the steel is very stiff, and $\sigma_{11} >> \sigma_{22}$ due to the dominance of bending. Hence the majority contribution to J arises from work at the ends. Since most of the energy stored in the steel is in the form of bending stress and changes little compared to the energy stored in the epoxy resin, we can write $J_1+J_{3a} \approx 0$ giving

$$J \approx \int_{0}^{H}\int_{0}^{\varepsilon_{11}} \sigma_{11(x_1=l)}\, d\varepsilon_{11}\, dx_{11}$$

In some situations J would be considered to be equivalent to the strain energy release rate G for the system. However, the work quantity calculated above is clearly not all available to drive fracture as significant plastic deformation has occurred in the epoxy resin.

A test of the degree to which a J-integral calculation may be considered valid is the extent to which its result is independent of the path along which it is calculated. J-integral calculations in a model of the adhesion test using a highly refined crack-tip mesh displayed very poor path independence, confirming that the technique is unsuitable for the system of interest. Therefore, in the FEM models, like the analytical model, an argument based on the elastic energy stored in uniformly deformed sections was employed in calculating Gc.